

Basis Adaptive Algorithm for Quantum Many-Body Systems on Quantum Computers

Anutosh Biswas,¹ Sayan Ghosh,¹ Ritajit Majumdar,² Mostafizur Rahaman,² and Manoranjan Kumar^{1,*}

¹*S.N. Bose National Centre for Basic Sciences, Kolkata 700106, India.*

²*IBM Quantum, IBM India Research Lab, Bengaluru, India.*

(Dated: December 16, 2025)

A new basis adaptive algorithm for hybrid quantum-classical platforms is introduced to efficiently find the ground-state (gs) properties of quantum many-body systems. The method addresses limitations of many algorithms, such as Variational Quantum Eigensolver (VQE) and Quantum Phase Estimation (QPE) etc by using shallow Trotterized circuits for short real-time evolution on a quantum processor. The sampled basis is then symmetry-filtered by using various symmetries of the Hamiltonian which is then classically diagonalized in the reduced Hilbert space. We benchmark this approach on the spin-1/2 XXZ chain up to 24 qubits using the IBM Heron processor. The algorithm achieves sub-percent accuracy in ground-state energies across various anisotropy regimes. Crucially, it outperforms the Sampling Krylov Quantum Diagonalization (SKQD) method, demonstrating a substantially lower energy error for comparable reduced-space dimensions. This work validates symmetry-filtered, real-time sampling as a robust and efficient path for studying correlated quantum systems on current near-term hardware.

I. INTRODUCTION

Quantum many-body effects in condensed matter systems are ubiquitous and especially, in condensed matter physics, this play a crucial role in giving rise to a variety of emergent quantum phases, including unconventional magnetism [1–3], superconductivity [4–6], quantum spin liquids [7–9], and entanglement-driven orders [10, 11]. However, studying the quantum many body systems remains intractable due to the exponential growth of the Hilbert-space dimension with system size. This exponential scaling makes exact solutions infeasible for most systems, while exactly solvable small systems suffer from significant finite-size effects, which hinder a true understanding of real materials [12–14]. Standard numerical approaches—such as exact diagonalization (ED)[14–16], quantum Monte Carlo [17–22], and tensor-network methods [23–26]—have provided important insights, but each suffers from inherent limitations. ED is restricted by small system sizes, quantum Monte Carlo is limited by the fermionic and frustrated sign problems [27, 28], and tensor-network methods struggle in regimes with strong entanglement or long correlation lengths [29].

Quantum computation offers a potential path forward by encoding many-body wavefunctions directly in quantum hardware. A variety of algorithms have been proposed for ground-state preparation and Hamiltonian simulation. The Variational Quantum Eigensolver (VQE) [30–34] is attractive for near-term hardware devices because it requires shallow circuits, but its performance is limited by optimization landscapes that become highly nonconvex for strongly correlated states [35]. Quantum Phase Estimation (QPE) [36, 37] can achieve high precision but demands deep, coherent circuits that are only practical on fault-tolerant quantum processors. Krylov

subspace methods [38], including Sampling Krylov Quantum Diagonalization (SKQD) [39], mitigate some depth requirements but often generate noisy or symmetry-violating subspaces, reducing accuracy. Imaginary-time evolution schemes [40, 41] involve effective nonunitary dynamics that must be approximated with ancilla-based circuits and are sensitive to noise. Real-time evolution approaches [42, 43] can be implemented using shallow Trotter circuits, but short-time evolution may not capture the dominant ground-state structure unless basis states are carefully selected and filtered.

These challenges motivate the development of a accurate basis adaptive algorithm for hybrid quantum-classical platform that generates compact, physically meaningful basis set while remaining compatible with present-day hardware. In this work, we introduce an algorithm in which reduced Hilbert space with only relevant bases are obtained using an efficient time evolution on a quantum computer. These bases are explicitly filtered to preserve key symmetries of the Hamiltonian, including conservation of total S^z and lattice reflection symmetry. The Hamiltonian is then diagonalized within this reduced Hilbert space to obtain the ground-state energy and wavefunction. Because the method naturally focuses on the low-energy sector, it avoids the heavy optimization overhead of VQE, the deep circuits required by QPE, and the noise-induced instabilities that may arise in SKQD. Its reliance on shallow Trotterized circuits also makes it practical for near-term hardware.

In this work we study the spin- $\frac{1}{2}$ XXZ chain to evaluate the performance of the algorithm. The XXZ model is an interesting model which exhibits a ferromagnetic phase $\Delta < -1$, a critical Tomonaga–Luttinger liquid for $-1 < \Delta \leq 1$, and an antiferromagnetic Néel-ordered phase for $\Delta > 1$ [44, 45]. These regimes differ markedly in their entanglement structure and quantum fluctuation strength, making the model an ideal benchmark. We implement our algorithm on IBM’s Heron quantum processor for system sizes up to 24 qubits and compare the

* manoranjan.kumar@bose.res.in

results with exact diagonalization and SKQD.

Our results demonstrate that the proposed approach achieves sub-percent accuracy in ground-state energies across a broad range of anisotropy values. It also reproduces spin–spin correlation functions with high fidelity and outperforms SKQD for comparable reduced-space dimensions. These findings indicate that symmetry-filtered, real-time sampling provides a robust and efficient pathway for studying correlated quantum systems on currently accessible quantum hardware.

This paper is divided into five sections. In the second section we discuss the model Hamiltonian and numerical approaches which are used to benchmark our results and in the third section our Basis-Adaptive (BA) algorithm of the quantum computation and various results are discussed in Section Four. We summarize all these results in the fifth section.

II. MODEL HAMILTONIAN AND NUMERICAL APPROACH

The spin- $\frac{1}{2}$ XXZ chain is described by the Hamiltonian

$$H = J \sum_{j=1}^L (S_j^x S_{j+1}^x + S_j^y S_{j+1}^y + \Delta S_j^z S_{j+1}^z), \quad (1)$$

where $S_j^\alpha = \frac{1}{2}\sigma_j^\alpha$ are spin-1/2 operators, and $J = 1$ sets the energy scale and antiferromagnetic nature of exchange, Δ as the anisotropy parameter controlling the interaction along the z-axis. In this work, we employ Exact Diagonalization (ED) to benchmark the results obtained from the BA algorithm for system sizes up to $N = 24$ [46]. Using these complementary numerical approaches, we compare the gs energy, spin–spin correlation functions, and fidelity of gs wavefunction obtained from BA algorithm and ED method. These comparisons serve as benchmarks for assessing the accuracy and performance of our Basis-Adaptive (BA) Algorithm.

III. BASIS ADAPTIVE ALGORITHM

For a given quantum system, the ground-state wavefunction can always be expressed as a linear combination of the computational basis states of the Hilbert space. If $\{|b_0\rangle, |b_1\rangle \dots |b_k\rangle \dots\}$ denotes a complete basis, then the ground state may be written as

$$|\psi_{\text{gs}}\rangle = \sum_k c_k |b_k\rangle. \quad (2)$$

In most physical systems, only a very small fraction of these basis states contribute significantly to the ground-state wavefunction, while the majority have negligible amplitudes i.e. $c_k \approx 0$. Therefore, it is natural to construct an approximate ground state using only the most

probable basis states (bitstrings),

$$|\psi_{\text{gs}}^A\rangle \approx \sum_{k \in \mathcal{S}}^{N_{SD}} c'_k |b_k\rangle, \quad (3)$$

where \mathcal{S} denotes the subset of N_{SD} number of basis states with significantly finite amplitudes c'_k . Our final goal is to get $|\psi_{\text{gs}}^A\rangle$, therefore, we begin with a very small set dominant basis states $\{|b_k\rangle\}$ and evolve them through a short time step, Δt . The short-time evolution of the approximate state can be written as

$$|\psi_{\text{gs}}^{A'}(\Delta t)\rangle = e^{-iH\Delta t} \sum_k a_k |b_k\rangle. \quad (4)$$

The time evolution is unitary operator and for small Δt , Taylor expansion of the time evolution operator has the following form,

$$e^{-iH\Delta t} \approx I - i\Delta t H + \frac{(i\Delta t H)^2}{2} + \mathcal{O}(\Delta t^3), \quad (5)$$

After a short-time Δt approximate state can be written as

$$|\psi_{\text{gs}}^{A'}(\Delta t)\rangle \approx \left[I - i\Delta t H + \frac{(i\Delta t H)^2}{2} + \dots \right] \sum_k a_k |b_k\rangle. \quad (6)$$

The evolved state may also be expanded in the exact eigenbasis $\{|\psi_n\rangle\}$ of the Hamiltonian,

$$|\psi_{\text{gs}}^{A'}(\Delta t)\rangle \approx \sum_n a'_n e^{-iE_n \Delta t} |\psi_n\rangle, \quad (7)$$

and re-expanding it back in the computational basis yields

$$|\psi_{\text{gs}}^{A'}(\Delta t)\rangle \approx \sum_{b'_k} a''_{k'} |b'_k\rangle. \quad (8)$$

The long time evolution naturally generates many additional basis states and the evolved wavefunction becomes function of various basis states which are generated through two-, four- or higher order spin flips, expanding the size of the truncated Hilbert space. To get a flavor of this we used spin flipped basis states for obtaining accurate gs of models in Ising limit of the Hamiltonian starting with antiferromagnetic Ising basis and the calculation is presented in the Supplementary Material (SM) [47]. It is shown that how the transverse anisotropy can be treated perturbatively and second and fourth order of contribution are just two spin flip or four spin flip terms. However, higher order of spin-flip process may generate all the basis states and these states may not be specifically relevant to only low-energy eigen-states of the Hamiltonian.

In this work, we are interested only in the gs, thus, we want to generate only those basis states of the Hilbert

space which are relevant to the gs. We follow an iterative algorithm [48], where, we start with only a few basis states which are most relevant for the gs of the Hamiltonian and the operation of Hamiltonian on these basis states very similar to the time evolution which generates many newly configuration. We now construct the Hamiltonian matrix in the newly expanded reduced Hilbert space and get gs wavefunction. The most probable basis states, i.e states with highest probability, are selected and these basis states are time evolved to form the expanded Hilbert space. This process is repeated till the gs energy is converged.

This method can be efficiently implemented on the Quantum Computer (QC) and basis states can be evolved with short time using the QC and the construction of the Hamiltonian matrix and gs wavefunction calculation is done on classical computer. In this work we develop a basis adaptive algorithm which used hybrid quantum and classical approach to solve the quantum many body model systems. The steps of the BA algorithm can be described below:

1. **Initialization:** We prepare a small set of representative bitstrings, $\{b_k^{(0)}\}$, which encode the dominant spin configurations contributing to the ground state of the Hamiltonian H . Each bitstring corresponds to a computational-basis state $|b_k^{(0)}\rangle$ within the Hilbert space of the system H . Unlike conventional wavefunction-based approaches, we treat each $|b_k^{(0)}\rangle$ as an independent sample wavefunction. The initial configurations can be chosen from the ground state of the Ising (axial) part of H or guided by the most probable basis states obtained from solution of small system size. For example, in the XXZ Hamiltonian (Eq. 1) with $J > 0$, the two relevant configurations are

$$|b_1^{(0)}\rangle = |\uparrow\downarrow\uparrow\downarrow\cdots\rangle, \quad |b_2^{(0)}\rangle = |\downarrow\uparrow\downarrow\uparrow\cdots\rangle.$$

2. **Time Evolution:** In the i -th iteration, each configuration $|b_k^{(i)}\rangle$ is evolved independently under the unitary operator $U(\Delta t) = e^{-iH\Delta t}$:

$$|b_k^{(i)'}\rangle = e^{-iH\Delta t} |b_k^{(i)}\rangle. \quad (9)$$

For the XXZ Hamiltonian,

$$H = \sum_j H_j, \quad H_j = \frac{1}{2} (S_j^+ S_{j+1}^- + S_j^- S_{j+1}^+) + \Delta S_j^z S_{j+1}^z. \quad (10)$$

Using the first-order Lie–Trotter decomposition,

$$e^{-iH\Delta t} \approx \prod_j e^{-iH_j\Delta t} + \mathcal{O}((\Delta t)^2), \quad (11)$$

each local term H_j acts on two neighboring spins, allowing the evolution to be implemented through

a sequence of two-qubit unitaries on a quantum circuit (see Fig. 1). The detailed construction of the circuit is discussed in the SM [47]. The same circuit is applied independently to each input bitstring $|b_k^{(i)}\rangle$, producing the evolved configurations $|b_k^{(i)'}\rangle$.

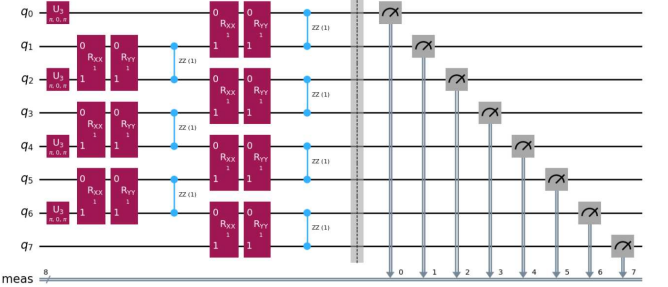


FIG. 1. Trotterized quantum circuit for the XXZ Hamiltonian in Eq. 1 based on the first-order **Lie–Trotter decomposition**. The bond exchange of Hamiltonian $H_k = J(X_k X_{k+1} + Y_k Y_{k+1}) + \Delta Z_k Z_{k+1}$ is decomposed into non-commuting parts H_{XY} and H_{ZZ} , whose time evolutions are implemented sequentially using R_{XX} , R_{YY} , and ZZ rotation gates. The single-qubit U_3 gates prepare the initial state, and the layered structure of R_{XX} , R_{YY} , and ZZ gates realizes one Trotter step of the evolution.

3. **Measurement, Union, and Symmetry Filtering:** In the third step, each evolved configuration $|b_k^{(i)'}\rangle$ is measured in the computational basis to obtain a sequence of bitstrings $\{b_k^{(i)'}\}$. The complete set of bitstrings generated from all evolved configurations is then combined to form their union,

$$\mathcal{B}^{(i)'} = \bigcup_k \{b_k^{(i)'}\}.$$

From this unified set $\mathcal{B}^{(i)'}$, we retain only those bitstrings that satisfy the required physical constraints — specifically, conservation of the total S^z component and the $U(1)$ symmetry of the Hamiltonian. Furthermore, we enforce reflection symmetry by including only those configurations (and their symmetry-related partners) that respect the reflection invariance of the Hamiltonian. The resulting symmetry-adapted set of bitstrings is denoted as $\{b_s^{(i)'}\}$, ensuring that the reduced subspace preserves both $U(1)$ and reflection symmetries.

4. **Hilbert-Space Reconstruction and Classical Diagonalization:** In the fourth step, the filtered and symmetrized bitstrings $\{b_s^{(i)'}\}$ define the reduced Hilbert space for the next iteration. Within this reduced subspace, we construct the Hamiltonian matrix corresponding to H and perform an exact diagonalization on a classical computer. The lowest eigenvalue and the associated eigenvector, denoted as E^i and $|\Psi^i\rangle$, respectively, represent the

approximate ground-state energy and wavefunction at the i -th iteration.

5. In the fifth step, if our ground state energy is converged then we calculate all the relevant quantity like correlation functions, spin density etc and exit or we construct updated wavefunction retaining m_i number of basis states which have highest probability C_i^2 in the ground state wavefunction. These most probable bases $\{b_m^i\}$ work as initial basis set for the next iteration $(i+1)^{th}$ and repeat the step two-five till the energy is converged. Typically, the dominant basis states contributing to the ground state are recovered within two iterations, leading to rapid convergence of the ground-state energy.

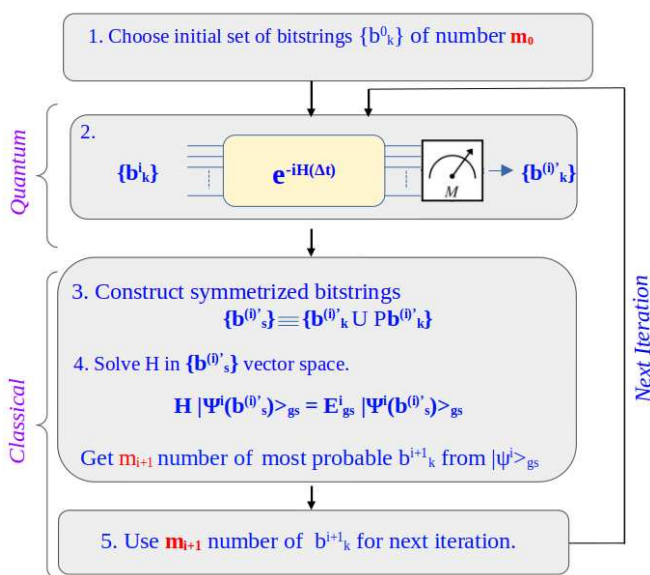


FIG. 2. Schematic workflow of the Basis Adaptive Algorithm. An initial set of m_0 bitstrings is evolved using the Trotterized time-evolution operator on a quantum device and measured to generate a new set of sampled bitstrings. These bitstrings are then expanded by adding symmetry-related configurations, forming a symmetrized subspace in which the Hamiltonian is classically diagonalized. The m_i most probable bitstrings from the resulting eigenstate are selected and used to define the basis set for the next iteration.

IV. RESULTS

In this section we present a detailed analysis of the performance of the proposed quantum-classical hybrid BA algorithm applied to a antiferromagnetic spin- $\frac{1}{2}$ XXZ Hamiltonian on a chain and we focus on the antiferromagnetic side. We start with only two initial basis states ($m_0 = 2$); $|b_1^0\rangle = |\uparrow\downarrow\uparrow\downarrow\uparrow\downarrow\dots\rangle$ and $|b_2^0\rangle = |\downarrow\uparrow\downarrow\uparrow\downarrow\dots\rangle$. The time evolution of these two basis states or bitstrings are done using IBM quantum hardware (Heron) for system sizes up to $N = 24$ qubits and we follow all the steps of

the BA algorithm. We notice that even for the second iteration of the BA algorithm the error of the gs energy is reduced to less than a percent. Therefore, all results are shown for the second iteration of algorithm and at the end of first iteration which start choosing only m_1 most probable basis obtained at the end of first iteration. We benchmark hybrid algorithm results against the exact diagonalization (ED) to evaluate the accuracy of gs energies, the fidelity F between the exact and wavefunctions calculated from the BA algorithm, and the reliability of spin-spin correlation functions. We also compare the energies with the Sampling Krylov Quantum Diagonalization (SKQD) method.

A. Analysis of the gs energy and fidelity

To generate the time-evolved state, we implemented a single-step first-order Trotterized evolution with a time step $\Delta t = 0.25$ [see Fig. 1]. The evolved state was repeatedly measured in the computational basis, and the collected bitstrings were post-selected to enforce two symmetries inherent to the XXZ Hamiltonian: first, conservation of the z-component of the total spin S^z and second, reflection symmetry of the spin chain. Enforcing symmetry at the sampling stage significantly stabilizes the reconstruction of the reduced Hilbert space and suppresses noise-induced leakage into symmetry-forbidden sectors.

For all the calculation presented in this work is done by constructing the Hamiltonian matrix in reduced dimension of Hilbert space m_{SD} at the end of 2^{nd} iteration of the BA algorithm and gs energy and wavefunctions are calculated. In Fig. 3 the percentage error in the gs energy as a function of the number of most probable bases in the second iteration m_1 is shown. The percentage error in gs energy is defined as, $\Delta E_{gs} = \frac{E_{gs}(BA) - E_{gs}(ED)}{E_{gs}(ED)} \times 100$ where $E_{gs}(BA)$ and $E_{gs}(ED)$ are total gs energy calculated from the BA algorithm and ED method respectively. ΔE_{gs} decreases rapidly as the number of basis states increases. For $m_1 = 96$ and ΔE_{gs} is reduced to approximately 1% and this accuracy is achieved only by recovering around 18% of the total Hilbert space after 2^{nd} iteration shown in Table I.

There are two factors which effect the generation of new basis set first the number of initial basis set at the beginning of $(i+1)^{th}$ iteration m_i and number of measurement shots M_s . Larger number of m_i help to generate the larger amount of basis states faster, whereas higher number of shots will generate new basis states, but these states may include from higher order of spin flips of original basis state. In Fig. 3 (a), we show the dependence of ΔE_{gs} on m_1 for two $M_s = 20K$ and $40K$ and $\Delta = 1.0$. Increasing m_1 expands dimension of relevant reduced Hilbert space at the second step and re-

sulting higher accuracy of energy as shown in Fig. 3 (a). The higher number of M_s lead to reducing sampling fluctuations, highlighting the importance of measurement statistics in the reconstruction process.

We also evaluate the gs fidelity F which is used to characterize the wavefunction accuracy and it can be defined as

$$F = \langle \psi_{gs}^{\text{BAA}} | \psi_{gs}^{\text{ED}} \rangle, \quad (12)$$

where $|\psi_{gs}^{\text{BAA}}\rangle$ and $|\psi_{gs}^{\text{ED}}\rangle$ are the gs wavefunctions obtained from BA algorithm and ED, respectively. The variation of fidelity with Δ is summarized in Table I. For all the cases the Fidelity is always more the 0.96 which indicates excellent accuracy of the wavefunction.

TABLE I. Subspace dimensions (SD), referring to the basis generated after the second iteration, percentage error in the ground-state energy (ΔE_{gs}), and fidelity (F) for $N = 24$ with $M_s = 40K$ and $m_1 = 96$. The total Hilbert space dimension is 2704156.

Δ	SD	ΔE_{gs}	F
1.0	469004	0.87%	0.96534
1.2	442005	0.64%	0.97404
1.4	498979	0.38%	0.98534

B. Dependence on anisotropy parameter Δ

To examine the performance of the algorithm for various physical parameter regimes, we computed the ground-state energy for several values of the anisotropy parameter $\Delta \geq 1$. Fig. 3 (b) displays the percentage deviation from ED for $\Delta = 1.0, 1.2, 1.4$, with various $m_1 = 16$ to 96 and $M_s = 40K$.

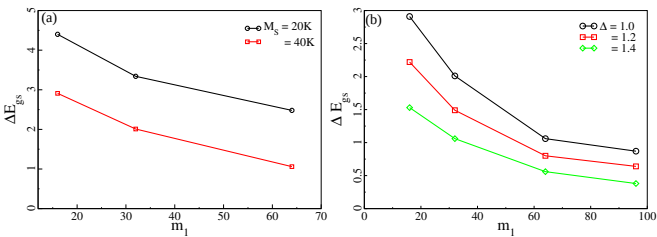


FIG. 3. (a) Percentage error in the ground-state energy as a function of the maximum number of retained basis states (m_1), shown for different values of M_s . Increasing m_1 systematically improves the ground-state accuracy. (b) Percentage error as a function of m_1 for several values of Δ , computed using $M_s = 40K$. The results highlight how enlarging the basis enhances the ground-state accuracy.

For the antiferromagnetic isotropic Heisenberg limit, $\Delta = 1.0$, strong quantum fluctuations lead to a broad distribution of basis states, therefore, isotropic system

shows highest energy fluctuation and error is less than 1% for $m_1 = 96$ as shown in Fig. 3 (b). Increasing the values of Δ the system gradually enters the Ising-dominated regime, where the longitudinal interaction term $\Delta S_i^z S_{i+1}^z$ dominates and transverse fluctuation decreases. In this regime, the ground state becomes increasingly classical and spin configuration is close to antiferromagnet. Consequently, the sampling-based reconstruction becomes more efficient, and the error in the ground-state energy systematically decreases. We also notice that $m_1 = 64$ is sufficient to get the energy error less than 1%. For $\Delta = 1.4$, the error falls well below 1%, demonstrating excellent performance deep in the Ising regime.

C. Spin-Spin Correlation Functions

Generally, error in global quantities like total energy tend to cancel out and give very good accuracy in the approximate method but local correlation accuracy are generally poor. Therefore we calculate the spin-spin correlation function correlation function $C(r)$ between two spins separated by a distance r , which provides valuable insight into the nature of magnetic ordering in the system. The correlation function is defined as

$$C(r) = \langle \vec{S}_i \cdot \vec{S}_{i+r} \rangle. \quad (13)$$

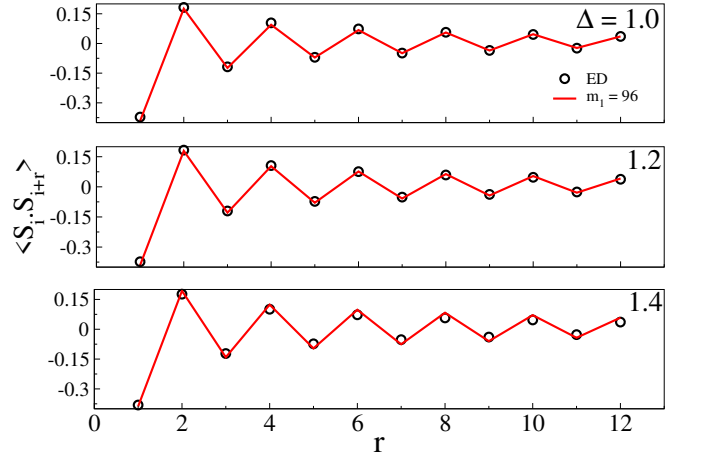


FIG. 4. For different Δ values correlation function is shown for 24 number of qubits with $M_s = 40K$.

Fig. 4 shows $C(r)$ for a system size $N = 24$ and several values of the anisotropy parameter Δ , computed using $M_s = 40K$ and $m_1 = 96$. In Fig. 4, the results obtained from exact diagonalization (ED, shown as circles) are compared with those from BA algorithm (shown as lines). For all values of Δ , the correlation functions exhibit excellent agreement with the ED benchmarks. The reliable reproduction of $C(r)$ over long distances indicates that the algorithm not only captures global energetic properties but also accurately reconstructs non-local corre-

lations, which are sensitive probes of the wavefunction structure.

D. Comparison with SKQD

To benchmark the efficiency and accuracy of our algorithm, we compared its performance with the Sampling-based Krylov Quantum Diagonalization (SKQD) method which is considered to be most efficient algorithm at present [39]. Table II summarizes the results for $\Delta = 1.0$ and $\Delta = 1.2$. At $\Delta = 1.0$, SKQD exhibits an error of 12.14% in the ground-state energy, whereas our approach yields a substantially lower error of 0.87%. The width of Trotter circuits of the BA algorithm is much shorter than SKQD, however, evolution of the most relevant basis states for the gs results in further generating the relevant basis states for the gs. Combined with explicit U(1) and reflection symmetry enforcement, this produces a compact, well-conditioned reduced space for the relevant energy state. The classical diagonalization step is therefore more stable and yields significantly improved accuracy for comparable subspace dimensions.

TABLE II. Comparison of Subspace Dimension (SD) and ΔE_{gs} between SKQD (with 6 Trotter steps) and our BA algorithm at $\Delta t = 0.25$ with $M_s = 40K$.

Δ	SD		ΔE_{gs}		ED Energy
	SKQD	BA algorithm	SKQD	BA algorithm	
1.0	39733	469004	12.14	0.87	-10.45378

V. SUMMARY

The challenge of simulating correlated quantum many-body systems stems from the exponential scaling of the Hilbert space. While quantum computation offers a path forward, existing algorithms like VQE are limited by

complex optimization landscapes, and QPE requires prohibitive circuit depth. We introduce an hybrid quantum-classical algorithm ,the BA algorithm' which overcomes above limitations by utilizing shallow Trotterized circuits for short and one step real-time evolution on a quantum processor and choosing the most relevant basis for the selected energy state. The resulting relevant basis of the reduced Hilbert space are then rigorously symmetry-filtered to enforce symmetry like conservation of longitudinal component of total spin and lattice reflection symmetry of the model Hamiltonian. Thereafter, classical computer diagonalizes the Hamiltonian within reduced Hilbert space to find the gs properties.

Benchmarking of the gs results for the spin-1/2 XXZ chain up to $N = 24$ qubits (on IBM's Heron) demonstrates the algorithm achieves sub-percent accuracy in ground-state energies across anisotropy values $\Delta \geq 1$. The error for the isotropic limit $\Delta = 1.0$ is 0.87%, which is much less from any existing algorithm. The method also accurately reproduces spin-spin correlation functions and outperforms Sampling Krylov Quantum Diagonalization (SKQD). This validates that symmetry-filtered, real-time quantum sampling offers a robust and efficient pathway for high-accuracy ground-state simulations on current near-term hardware.

VI. ACKNOWLEDGMENT

We thank Dr. Richa Goel and Mr. Md. Sanowaz Molla for their fruitful discussions. AB acknowledge the financial support from DST-India. SG thanks DST-Inspire for financial support. We acknowledge National Supercomputing Mission (NSM) for providing computing resources of 'PARAM RUDRA' at S.N. Bose National Centre for Basic Sciences, which is implemented by C-DAC and supported by the Ministry of Electronics and Information Technology (MeitY) and Department of Science and Technology (DST), Government of India.

[1] L. Balents, Spin liquids in frustrated magnets, *Nature* **464**, 199 (2010).
[2] R. Moessner and A. P. Ramirez, Geometrical frustration, *Physics Today* **59**, 24 (2006).
[3] J. S. Gardner, M. J. Gingras, and J. E. Greidan, Magnetic pyrochlore oxides, *Rev. Mod. Phys.* **82**, 53 (2010).
[4] P. A. Lee, N. Nagaosa, and X.-G. Wen, Doping a mott insulator: Physics of high-temperature superconductivity, *Rev. Mod. Phys.* **78**, 17 (2006).
[5] D. J. Scalapino, A common thread: The pairing interaction for unconventional superconductors, *Rev. Mod. Phys.* **84**, 1383 (2012).
[6] B. Keimer, S. A. Kivelson, M. R. Norman, S.-i. Uchida, and J. Zaanen, From quantum matter to high-temperature superconductivity in copper oxides, *Nature* **518**, 179 (2015).
[7] L. Savary and L. Balents, Quantum spin liquids: a review, *Rep. Prog. Phys.* **80**, 016502 (2017).
[8] Y. Zhou, K. Kanoda, and T.-K. Ng, Quantum spin liquid states, *Rev. Mod. Phys.* **89**, 025003 (2017).
[9] S. Yan, D. A. Huse, and S. R. White, Spin-liquid ground state of the $s=1/2$ kagome heisenberg antiferromagnet, *Science* **332**, 1173 (2011).
[10] P. W. Anderson, The resonating valence bond state in La_2CuO_4 and superconductivity, *Science* **235**, 1196 (1987).
[11] M. Imada, A. Fujimori, and Y. Tokura, Metal-insulator transitions, *Rev. Mod. Phys.* **70**, 1039 (1998).
[12] G. D. Mahan, *Many Particle Physics*, *Third Edition* (Plenum, New York, 2000).
[13] A. L. Fetter and J. D. Walecka, *Quantum Theory of Many-Particle Systems* (McGraw-Hill, Boston, 1971).

[14] A. W. Sandvik, Computational studies of quantum spin systems, in *AIP Conference Proceedings*, Vol. 1297 (American Institute of Physics, 2010) pp. 135–338.

[15] H. Lin, Exact diagonalization of quantum-spin models, *Physical Review B* **42**, 6561 (1990).

[16] P. Nataf and F. Mila, Exact diagonalization of heisenberg su (n) models, *Physical review letters* **113**, 127204 (2014).

[17] W. M. Foulkes, L. Mitas, R. Needs, and G. Rajagopal, Quantum monte carlo simulations of solids, *Reviews of Modern Physics* **73**, 33 (2001).

[18] L. Pollet, Recent developments in quantum monte carlo simulations with applications for cold gases, *Reports on progress in physics* **75**, 094501 (2012).

[19] J. Gubernatis, N. Kawashima, and P. Werner, *Quantum Monte Carlo Methods* (Cambridge University Press, 2016).

[20] A. W. Sandvik and J. Kurkijärvi, Quantum monte carlo simulation method for spin systems, *Physical Review B* **43**, 5950 (1991).

[21] D. Ceperley and B. Alder, Quantum monte carlo, *Science* **231**, 555 (1986).

[22] R. R. d. Santos, Introduction to quantum monte carlo simulations for fermionic systems, *Brazilian Journal of Physics* **33**, 36 (2003).

[23] S. Montangero, E. Montangero, and Evenson, *Introduction to tensor network methods* (Springer, 2018).

[24] M. C. Bañuls, Tensor network algorithms: A route map, *Annual Review of Condensed Matter Physics* **14**, 173 (2023).

[25] S.-J. Ran, E. Tirrito, C. Peng, X. Chen, L. Tagliacozzo, G. Su, and M. Lewenstein, *Tensor network contractions: methods and applications to quantum many-body systems* (Springer Nature, 2020).

[26] M. Fishman, S. White, and E. M. Stoudenmire, The itensor software library for tensor network calculations, *Sci-Post Physics Codebases* , 004 (2022).

[27] G. Pan and Z. Y. Meng, Sign problem in quantum monte carlo simulation, *arXiv preprint arXiv:2204.08777* (2022).

[28] M. Troyer and U.-J. Wiese, Computational complexity and fundamental limitations to fermionic quantum monte carlo simulations, *Physical review letters* **94**, 170201 (2005).

[29] U. Schollwöck, The density-matrix renormalization group, *Rev. Mod. Phys.* **77**, 259 (2005).

[30] J. Tilly, H. Chen, S. Cao, D. Picozzi, K. Setia, Y. Li, E. Grant, L. Wossnig, I. Rungger, G. H. Booth, *et al.*, The variational quantum eigensolver: a review of methods and best practices, *Physics Reports* **986**, 1 (2022).

[31] A. Kandala, A. Mezzacapo, K. Temme, M. Takita, M. Brink, J. M. Chow, and J. M. Gambetta, Hardware-efficient variational quantum eigensolver for small molecules and quantum magnets, *nature* **549**, 242 (2017).

[32] J.-G. Liu, Y.-H. Zhang, Y. Wan, and L. Wang, Variational quantum eigensolver with fewer qubits, *Physical Review Research* **1**, 023025 (2019).

[33] Y. Zhang, L. Cincio, C. F. Negre, P. Czarnik, P. J. Coles, P. M. Anisimov, S. M. Mniszewski, S. Tretiak, and P. A. Dub, Variational quantum eigensolver with reduced circuit complexity, *npj Quantum Information* **8**, 96 (2022).

[34] A. Peruzzo, J. McClean, P. Shadbolt, M.-H. Yung, X.-Q. Zhou, P. J. Love, A. Aspuru-Guzik, and J. L. O'brien, A variational eigenvalue solver on a photonic quantum processor, *Nature communications* **5**, 4213 (2014).

[35] J. R. McClean, S. Boixo, V. N. Smelyanskiy, R. Babbush, and H. Neven, Barren plateaus in quantum neural network training landscapes, *Nature communications* **9**, 4812 (2018).

[36] A. Kitaev, Quantum measurements and the abelian stabilizer problem, *arXiv:quant-ph/9511026* (1995).

[37] M. A. Nielsen and I. L. Chuang, *Quantum Computation and Quantum Information* (Cambridge University Press, 2000).

[38] N. Yoshioka, M. Amico, W. Kirby, P. Jurcevic, A. Dutt, B. Fuller, S. Garion, H. Haas, I. Hamamura, A. Ivrii, *et al.*, Krylov diagonalization of large many-body hamiltonians on a quantum processor, *Nature Communications* **16**, 5014 (2025).

[39] M. M. et al., Hamiltonian simulation with krylov-space methods, *PRX Quantum* **2**, 040314 (2021).

[40] M. M. et al., Determining eigenstates and thermal states on a quantum computer using quantum imaginary time evolution, *Nat. Phys.* **16**, 205 (2020).

[41] S. M. et al., Variational ansatz-based quantum simulation of imaginary time evolution, *npj Quantum Inf.* **5**, 75 (2019).

[42] A. M. C. et al., Toward the first quantum simulation with quantum speedup, *PNAS* **115**, 9456 (2018).

[43] E. Campbell, Random compiler for fast hamiltonian simulation, *Phys. Rev. Lett.* **123**, 070503 (2019).

[44] T. Giamarchi, *Quantum Physics in One Dimension* (Oxford University Press, 2003).

[45] M. Takahashi, *Thermodynamics of One-Dimensional Solvable Models* (Cambridge University Press, 1999).

[46] A. W. Sandvik, Computational studies of quantum spin systems, *AIP Conference Proceedings* **1297**, 135 (2010), https://pubs.aip.org/aip/acp/article-pdf/1297/1/135/11407753/135_1.online.pdf.

[47] See Supplemental Material for providing the detailing of the trotterized quantum circuits and perturbation analysis in relation to the main text.

[48] S. S. Rahaman, S. Haldar, and M. Kumar, Machine learning approach to study quantum phase transitions of a frustrated one dimensional spin-1/2 system, *Journal of Physics: Condensed Matter* **35**, 115603 (2023).

Basis Adaptive Algorithm for Quantum Many-Body Systems on Quantum Computers

Anutosh Biswas,¹ Sayan Ghosh,¹ Ritajit Majumdar,² Mostafizur Rahaman,² and Manoranjan Kumar^{1,*}

¹*S.N. Bose National Centre for Basic Sciences, Kolkata 700106, India.*

²*IBM Quantum, IBM India Research Lab, Bengaluru, India.*

(Dated: December 16, 2025)

In this Supplementary Material, we provide detailed derivations, circuit constructions, and supporting theoretical explanations that complement the results presented in the main text. The contents are organized as follows:

- S1.** Trotterized quantum circuit for the XXZ Hamiltonian, including the construction of the unitary operator and its implementation using elementary gates.
- S2.** Decomposition of the nearest-neighbour XXZ Hamiltonian into XY and ZZ parts and the resulting Lie–Trotter factorization.
- S3.** Implementation of the R_{XX} , R_{YY} , and ZZ rotation gates, along with their hardware-native decompositions.
- S4.** Role of the Trotter circuit in the basis-adaptive algorithm and the scheme for sampling and symmetry-filtering computational basis states.
- S5.** Perturbative analysis of the XXZ Hamiltonian in the Ising limit ($\Delta \gg 1$), including second- and fourth-order corrections and the dominance of low spin-flip sectors.
- S6.** Summary of the key findings from the circuit construction and perturbative arguments.

S1. TROTTERIZED QUANTUM CIRCUIT FOR THE XXZ HAMILTONIAN

In the Basis-Adaptive (BA) algorithm described in the main text, the central quantum subroutine is the application of the unitary operator

$$U(\Delta t) = e^{-iH\Delta t},$$

to each basis configuration used as an independent sample wavefunction. This supplementary note explains the construction of the Trotterized quantum circuit that implements $U(\Delta t)$ for the XXZ Hamiltonian. A representative circuit is shown in Fig. 1.

S2. Decomposition of the XXZ Hamiltonian

The nearest-neighbour XXZ Hamiltonian is

$$H = \sum_j H_j, \quad H_j = J(S_j^x S_{j+1}^x + S_j^y S_{j+1}^y) + \Delta S_j^z S_{j+1}^z.$$

Each local term naturally separates into two non-commuting pieces:

$$H_j = H_{XY}^{(j)} + H_{ZZ}^{(j)},$$

where

$$H_{XY}^{(j)} = J(X_j X_{j+1} + Y_j Y_{j+1}), \quad H_{ZZ}^{(j)} = \Delta Z_j Z_{j+1}.$$

* manoranjan.kumar@bose.res.in

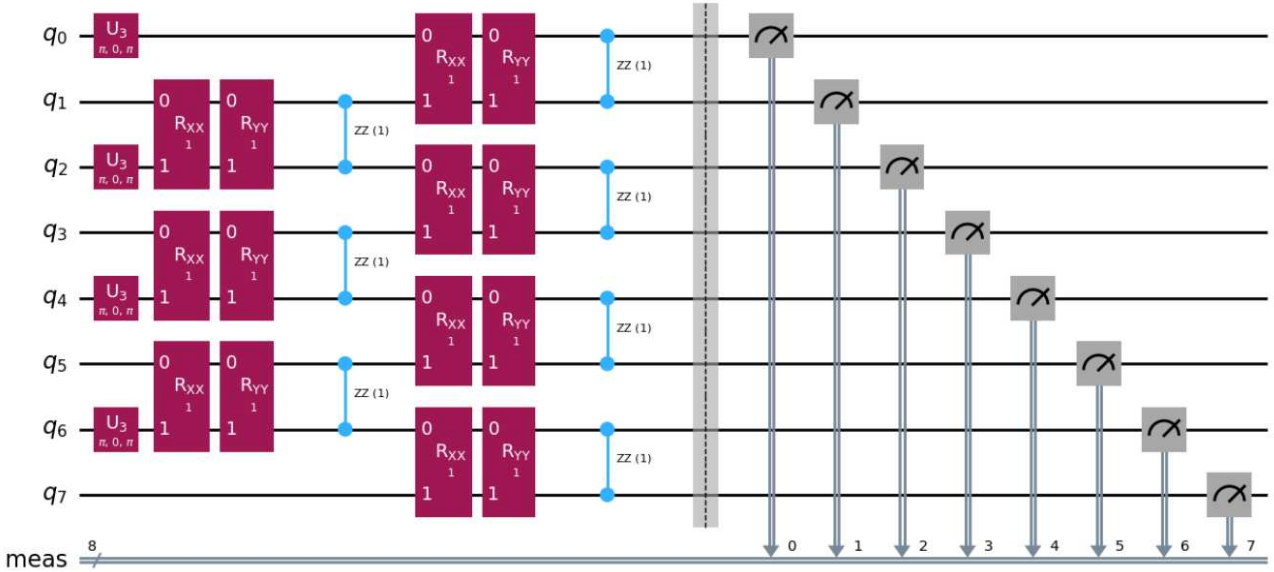


FIG. 1: Trotterized quantum circuit implementing one Trotter step of the XXZ Hamiltonian (Eq. (1)) using the first-order Lie–Trotter decomposition. The R_{XX} , R_{YY} , and ZZ rotation gates implement the XY -exchange and Ising interactions on each bond. Initial single-qubit U_3 rotations prepare the input computational-basis configuration.

Because the two parts do not commute, $[H_{XY}^{(j)}, H_{ZZ}^{(j)}] \neq 0$, the exact evolution operator is approximated using the first-order Lie–Trotter formula:

$$e^{-iH\Delta t} \approx \prod_j e^{-iH_{XY}^{(j)}\Delta t} e^{-iH_{ZZ}^{(j)}\Delta t} + \mathcal{O}((\Delta t)^2). \quad (1)$$

This factorization directly determines the layered structure of the quantum circuit.

S3. Implementation Using Entangling Gates

(a) XY exchange: R_{XX} and R_{YY} gates

For each bond $(j, j+1)$, the XY part evolves under

$$e^{-iH_{XY}^{(j)}\Delta t} = e^{-iJ\Delta t X_j X_{j+1}} e^{-iJ\Delta t Y_j Y_{j+1}}.$$

The corresponding two-qubit rotations are implemented using

$$R_{XX}(\theta) = e^{-i\frac{\theta}{2}X \otimes X}, \quad R_{YY}(\theta) = e^{-i\frac{\theta}{2}Y \otimes Y},$$

with rotation angle

$$\frac{\theta}{2} = J\Delta t.$$

Sequential application of R_{XX} and R_{YY} realizes the complete XY exchange for one Trotter slice.

(b) Ising term: ZZ rotation

The longitudinal interaction contributes

$$e^{-iH_{ZZ}^{(j)}\Delta t} = e^{-iJ\Delta\Delta t Z_j Z_{j+1}} \equiv ZZ(\phi),$$

with

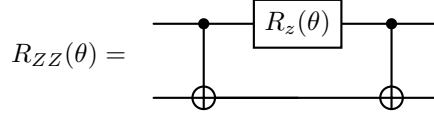
$$\frac{\phi}{2} = J \Delta \Delta t.$$

Most hardware platforms support $ZZ(\theta)$ natively, or via a controlled-phase gate decomposition.

(d) *Trotter Layer: Gate Decomposition*

Their decompositions into basis gates are:

a. *Decomposition of $R_{ZZ}(\theta)$:*



b. *Decomposition of $R_{XX}(\theta)$:*

$$R_{XX}(\theta) = (H \otimes H) R_{ZZ}(\theta) (H \otimes H)$$

c. *Decomposition of $R_{YY}(\theta)$:*

$$R_{YY}(\theta) = (R_x(\frac{\pi}{2}) \otimes R_x(\frac{\pi}{2})) R_{ZZ}(\theta) (R_x(-\frac{\pi}{2}) \otimes R_x(-\frac{\pi}{2}))$$

(c) *Full Trotter layer*

One complete Trotter layer thus consists of:

- R_{XX} rotations on all even bonds,
- R_{YY} rotations on all even bonds,
- ZZ rotations on all even bonds,
- followed by the same three gates on odd bonds.

S4. Role of the Circuit in the Basis-Adaptive Algorithm

Each computational-basis configuration $|b_k^{(i)}\rangle$ is treated as an independent sample wavefunction. For each such sample, the Trotter circuit implements

$$|b_k^{(i)'}\rangle = U(\Delta t) |b_k^{(i)}\rangle.$$

The measurements from all samples are collected to form the union set of bitstrings. Crucially:

- The full wavefunction is *never reconstructed* on hardware.
- Only the sampled computational-basis outputs are retained.
- Symmetry filtering enforces conservation of total S^z (U(1) symmetry) and reflection invariance.

The filtered set defines the reduced Hilbert subspace for the next iteration, in which we perform an exact diagonalization to obtain the approximate ground state.

S5. XXZ Hamiltonian in weak perturbation limit

To understand the underlying mechanism, we consider the Hamiltonian H given in Eq. 1 of the main text. For large values of Δ , the model reduces to the pure Ising limit, and the transverse exchange terms can be treated as a small perturbation. The Hamiltonian can therefore be written as

$$H = \sum_i S_i^z S_{i+1}^z + \gamma \sum_i \frac{1}{2} (S_i^+ S_{i+1}^- + S_i^- S_{i+1}^+) ,$$

where $\gamma = 1/\Delta$. In the Ising limit ($\gamma \rightarrow 0$), the ground state $|\alpha\rangle$ and one of the two-spin-flip excited states $|\alpha'\rangle$ are

$$|\alpha\rangle = |\uparrow\downarrow\uparrow\downarrow\cdots\rangle, \quad |\alpha'\rangle = |\uparrow\downarrow\uparrow\uparrow\downarrow\downarrow\cdots\rangle.$$

The energy of the Ising ground state is

$$E_0 = -\frac{N}{4},$$

while the two-spin-flip excitation has energy

$$E_0^{\alpha'} = -\frac{N}{4} + 1 = -\frac{1}{4}(N - 4).$$

The second-order correction to the ground-state energy arises from these two-spin-flip states:

$$\Delta E^{(2)} = - \sum_{\alpha'} \frac{|\langle \alpha' | H' | \alpha \rangle|^2}{E^{\alpha'} - E^{\alpha}}.$$

Since there are N such states, this simplifies to

$$\Delta E^{(2)} = -N \left(\frac{1}{2} \gamma \right)^2 = -\frac{N}{4} \gamma^2.$$

At fourth order, contributions come from states involving four spin flips. On a periodic chain, there are $N(N-1)/2$ such configurations, giving

$$\Delta E^{(4)} \propto \frac{(N-1)N}{2} \gamma^4.$$

Thus, for small γ , only the two-spin-flip and four-spin-flip sectors contribute significantly to the perturbative energy, while higher-order flip processes are negligible. This implies that during time evolution, the irrelevant high-order spin-flip sectors may be discarded at each step to retain only the physically relevant degrees of freedom. The percentage error in gs energy is defined as, $\Delta E_{gs} = \frac{|E_{gs}(\text{Perturbative}) - E_{gs}(ED)|}{E_{gs}(ED)} \times 100$.

TABLE I: Comparison of exact ground-state energy and perturbative energy for different γ values

Δ	Exact $E_{gs}(ED)$	Perturbative E_{gs}	ΔE_{gs}
0.1	-6.05985	-6.06	0.0025
0.05	-6.0149	-6.015	0.0016

S6. Summary

The Trotterized circuit in Fig. 1 efficiently encodes the XY and ZZ interactions of the XXZ Hamiltonian using native R_{XX} , R_{YY} , and ZZ gates. This circuit forms the core quantum subroutine of the basis-adaptive hybrid algorithm, allowing us to sample physically relevant configurations while avoiding the exponential complexity of a full wavefunction representation.